Diyala Journal of Engineering Sciences

Journal homepage: https://djes.info/index.php/djes

ISSN: 1999-8716 (Print); 2616-6909 (Online)

High-Performance Fuzzy Fractional-Order PID-Based Control Strategy for Grid-Tied Photovoltaic Systems with Active Power Filtering Capability

Salem Hafsia[1], Mohamed Toufik Benchouia[1], Habib Benbouhenni[2*], Abdessmad Milles[3], Amel Terki[1], Nicu Bizon[4]

[1]LGEB Laboratory, Department of Electrical Engineering, University of Biskra, Biskra 07000, Algeria
[2]Department of Electrical Engineering, Faculty of Technology, Hassiba Benbouali University of Chlef, Chlef, Algeria
[3]LPMRN Laboratory, Department of Electromechanics, Faculty of Technolog, University Mohamed El Bachir El Ibrahimi, Bordj Bou Arreridj 34030, Algeria
[4]The National University of Science and Technology POLITEHNICA Bucharest, Pitești University Centre, 110040 Pitesti, Romania

ARTICLE INFO

Article history:
Received: 02/11/2025.
Revised: 09/01/2026.
Accepted: 23/01/2026
Available online 15/03/2026

Keywords:
Fuzzy fractional-order proportional-integral derivative controller
Photovoltaic system
Maximum power point tracking
Space vector modulation
Synchronous reference frame
Fuzzy logic control

ABSTRACT

Currently, meeting grid standards for grid-connected photovoltaic (PV) solar power systems is a major challenge, particularly in terms of energy quality under conditions of non-linear loads, fluctuations in solar radiation, and parameter uncertainties. Conventional strategies based on proportional–integral–derivative (PID) regulators often suffer from limited robustness, higher total harmonic distortion (THD) of current, and noticeable fluctuations in voltage and power. To address these limitations, this work proposes a high-performance control strategy based on a fuzzy fractional-order PID (FFOPID) controller for a grid-connected PV system with efficient energy filtering capability. The proposed approach combines the robustness of fuzzy logic with the flexibility and memory characteristics of fractional-order control to regulate the DC-link voltage, ensure a unity power factor, reduce THD, and enhance dynamic performance. A systematic design methodology is developed to determine and optimize the FFOPID parameters. The studied system includes a PV array, a two-level inverter using space vector modulation, an inductive filter, a nonlinear load, and the utility grid. The proposed method is validated through MATLAB simulations and compared with the PI approach. Results demonstrate that the FFOPID significantly improves the overall system performance. In particular, the THD of the grid current is reduced from 4.05% with the PI to 0.63% with the proposed method. In addition, DC-link voltage fluctuations are minimized, and power oscillations are effectively suppressed. Stable operation is also maintained under sudden variations in solar irradiance and load conditions, confirming the effectiveness of the proposed approach for advanced grid-connected PV systems requiring high power quality.

1. INTRODUCTION

The future production of electrical power (EP) poses a significant challenge for countries worldwide, as it is a pivotal catalyst for global economic advancement. However, conventional power generation based on coal, oil, and natural gas contributes substantially to carbon emissions and environmental pollution [1]. In response to these challenges, many governments are increasingly integrating distributed energy resources (DERs) based on renewable energy (RE) technologies into the grid. These sources, such as solar and wind energy, offer a sustainable and clean alternative. Nevertheless, their intermittent nature and the widespread use of non-linear power electronic interfaces introduce significant power quality (PQ) issues, including harmonic distortion and grid instability [2,3]. Addressing these technical challenges is therefore essential to ensure the reliable and efficient operation of modern power systems with high renewable penetration. The accelerated processes

* Corresponding author's E-mail: habib0264@gmail.com
DOI: 10.24237/djes.2026.19104

of industrialization, urbanization, and globalization that characterize the contemporary era have precipitated a marked escalation in energy demand, giving rise to a discernible increase in the costs associated with energy production and consumption [2]. This overreliance on conventional energy sources, which are rapidly depleting, is inadequate to satisfy the escalating energy demands. Among the RE sources, solar energy has emerged as a prominent solution, having been adopted extensively and demonstrating minimal environmental impact. It has a substantial presence in a wide range of applications in the present day [3].

DERs based on photovoltaic (PV) systems are recognized as one of the most abundant available resources globally. They are regarded as a highly promising technology due to their high operational reliability, efficiency, and significant potential capacity [4]. Moreover, they are characterized by their pollution-free nature, a feature that has recently garnered considerable attention and has prompted researchers worldwide to develop improved methods to enhance PV systems.

In the contemporary era, the demand for EP is on the rise, owing to the proliferation of electronic energy interfaces across all levels of power generation, from the primary to the final consumption levels, including industrial and domestic sectors [5]. It is acknowledged that power generation systems derived from RE sources exhibit various defects, including but not limited to: impaired PQ, deterioration of the power factor, augmented power loss, and premature obsolescence of equipment. The efficacy of the control strategy employed is of paramount importance to the quality of the output power and the durability of the generation system [6]. Passive filters have been proposed to address the harmonic problem and correct the power factor. They have proven effective in reducing the overall total harmonic distortion (THD) of the current, thus limiting the negative effects and risks associated with high-current ripple. However, their successful implementation requires a thorough understanding of the electrical grid to avoid resonance problems. Furthermore, active filters offer a flexible alternative capable of accommodating the increasing use of electronic transformers. Unlike passive filters, active filters can adapt to changes in load conditions without requiring detailed information about the connected grid [7, 8].

The maximum power point (MPP) is identified by the MPP tracking (MPPT) controller through the transmission of the appropriate duty cycle (D) to the pulse width modulation (PWM) stage. The PWM stage directly governs the switching states of the DC-to-DC boost converter. The extant literature delineates a variety of algorithms and techniques, with MPPT methods generally classified into two distinct categories: intelligent and traditional approaches. Among traditional methods, the incremental conductance (IC) and perturb and observe (P&O) algorithms are the most popular due to their simplicity, intuitive operation, and relatively good performance [9]. Other methods, such as short circuit current (SCC) and open circuit voltage (OCV), have been developed to expedite the MPPT process by circumventing the minor, gradual alterations characteristic of the proportional-integral (PI) controller and the IC method. SCC demonstrates greater responsiveness to fluctuating weather conditions in comparison to OCV; however, both methods are constrained by the necessity of shorting or opening the PV circuit to ascertain their ratios [10]. While traditional methods offer certain advantages, they are susceptible to steady-state oscillations and may encounter difficulties in identifying the global maximum due to the non-linear characteristics of PV resources [11, 12]. Despite their benefits, traditional methods can exhibit steady-state oscillations and frequently fail to detect the global maximum, a consequence of the non-linear nature of PV systems. To address the aforementioned limitations, a variety of computational intelligence algorithms have been developed. These include artificial neural networks (ANN) [13, 14], fuzzy logic control (FLC) [15-16], genetic algorithms (GAs) [17, 18], particle swarm optimization (PSO) [19], grey wolf optimization (GWO) [20], and the yellow saddle goatfish algorithm (YSGA) [21]. Despite their demonstrated efficacy in a range of climates, the intricacy of these intelligent methods poses significant challenges to their practical implementation. To circumvent the limitations of usual methodologies, an indirect approach has been put forth, entailing the incorporation of an ancillary control layer for the generation of the duty cycle. Instead of directly generating the duty cycle, this method produces a reference voltage or current for a closed-loop regulator, which then adjusts the control signal accordingly [22]. Therefore, the rate of convergence to the MPP is contingent upon the efficacy of the control design.

In recent years, an active power filter (APF) has emerged as a novel PQ solution that aims to mitigate THDs, enhance power factor, and stabilize voltage fluctuations in electrical systems [23, 24]. A two-level APF constitutes a type of power filter that is frequently employed to reduce THD and enhance PQ in electrical systems [25]. This particular filter utilizes a voltage source inverter (VSI) to generate a current that counterbalances the harmonic current present within the system. A two-level APF exhibits several advantages and disadvantages. Among its merits are

high efficiency, rapid response time, and an enhanced power factor.

The primary challenge in APF control often lies in the regulation of the DC bus voltage. In the extant literature, proportional or PI regulators are frequently employed for current control [26, 27]. However, the implementation of PI regulators in filtration systems can result in various issues, particularly when system parameters change or a problem occurs with the load, leading to a decline in current quality. In addition to PI control, other techniques are recommended in some sources. These include resonant and multi-resonant controllers [28, 29]. However, achieving a balance between a satisfactory dynamic response and zero steady-state error (SSE), particularly in harmonic control, is often challenging with these controllers. An alternative approach involves the utilization of nonlinear controllers, which are more aptly suited to the variable structure characteristic of power converters. Among these, sliding mode controllers (SMCs) have been demonstrated to ensure a very fast dynamic response and zero SSE with a high degree of reliability [30]. Hysteresis current control, a particular instance of SMC [23], as well as synergetic control (SC) [31] and the super-twisting algorithm (STA) [32], have exhibited their efficacy in numerous studies [33, 34]. Nevertheless, the primary disadvantage of these strategies is their random switching frequency. Furthermore, these nonlinear strategies are susceptible to a phenomenon referred to as "chattering," which impedes their efficacy in control applications. This issue is not present with the SC-STA [35], as the output control signal is smooth and can be modulated at a fixed frequency. This strategy was initially implemented to regulate a WE generation system. In comparison to SMC, SC, and STA have been proposed as solutions to mitigate the chattering problem inherent in the SMC method [36].

FLC is regarded as one of the simplest and most adaptive intelligent control techniques for PV inverter systems, offering enhanced performance in terms of response time, settling time, and robustness against parameter uncertainties and load variations [37, 38]. In contrast to usual linear regulators, the FLC method does not necessitate an exact mathematical model and can effectively address system nonlinearities. In [39], an FLC system was applied to modify the parameters of conventional PI controllers in grid-connected APF. This approach resulted in smoother power and current responses with reduced overshoot compared to traditional controllers. However, the multi-functionality of the grid-connected converter was not explored. In a similar vein, [40] employed FLC to enhance power injection in voltage source converters (VSC) when interfaced with distributed generation (DG). To this end, two Mamdani-type FLCs were employed to regulate the reactive and active power (*Qs* and *Ps*) of the converter. A time-domain simulation, in conjunction with a black box optimization instrument, was employed to refine the fuzzy set parameters. The remaining FLC parameters were selected through a process of trial and error. The findings suggested that the utilization of FLC resulted in a marginal enhancement in power and voltage overshoot when compared to conventional controllers. This paper proposes a novel control system to optimize the operational performance of an efficient filter. The aim is to create a robust and high-performance control system to improve power and current quality. The primary contribution of this study is the integration of FL and fractional-order proportional-integral derivative (FOPID) to formulate a control system that exhibits both user-friendliness and exceptional robustness. The novel method of fuzzy FOPID (FFOPID) control has been introduced as a novel approach for regulating generation systems based on PV-SAPF. In the FFOPID-controlled SAPF system, the regulation of grid power components is achieved through the adjustment of specific elements within the SAPF converter circuit. The gains of the designed approach were determined by the genetic algorithm. Using this algorithm allows for significant improvements in performance and robustness. The use of this algorithm is also considered one of the paper's key contributions. Consequently, the PV converter is designated as the control output variable. The work presented in this paper differs from several other works [41-44] in terms of controller type, performance, durability, etc. Table 1 compares the designed approach with some research papers, providing a clear picture of the work and its significance in the field of energy and control. A significant benefit of this proposed control method is its independence from the system's mathematical model, enabling it to attain optimal results even in the presence of changing system parameters. The primary objectives of this study can be outlined as follows:

- The following section will introduce a new control that functions independently of system parameters. This control is characterized by its ease of use and high performance, which are its primary features.
- The FFOPID controller has been engineered to improve the performance of the PV system.
- It is imperative to minimize the THD value of the grid current.
- It is imperative to minimize the overshoot and SSE values of the *Ps* and *Qs*.
- The performance and efficiency of the new algorithm were compared to those of the usual methods through a numerical analysis. This analysis was conducted under various operating conditions.

The remaining components of the work are organized as follows: The second section of the text provides a comprehensive overview of the modeling process and the proposed system design. In Section 3, the proposed FFOPID technique is introduced. As delineated in Section 4, the proposed power control strategy is outlined in detail. In Section 5, the results of the proposed energy command are presented on the simulation platform. These results are then compared and analyzed with the PI control.

2. SYSTEM DESCRIPTION AND MODELING

The utility grid is designed to function as a sinusoidal voltage source with series short circuit impedances. The representation of this phenomenon is illustrated in Figure 1, which depicts the implementation of three-phase electromotive forces in series with these impedances. A nonlinear load is connected to the utility grid via intermediate line impedances (L_l, R_l) on the right side of the system. The load in question consists of an uncontrolled 3-phase rectifier that supplies a load (L_d, R_d) on its DC side. The figure in question also illustrates a DC-DC boost converter, which facilitates the integration of the PV generator with the grid through a VSI. The inverter, which is connected in parallel at the point of common coupling (PCC), functions as both a PV inverter and a shunt APF (SAPF). The SAPF is often controlled as a current generator. To guarantee that the grid current remains purely sinusoidal, the APF introduces unbalanced currents that are equal and in phase opposition to those absorbed by the nonlinear load. In essence, the APF functions to impede the circulation of disturbance currents generated by the nonlinear load through the grid impedances. This results in the drawing of pure sinusoidal and balanced total currents from the AC main.

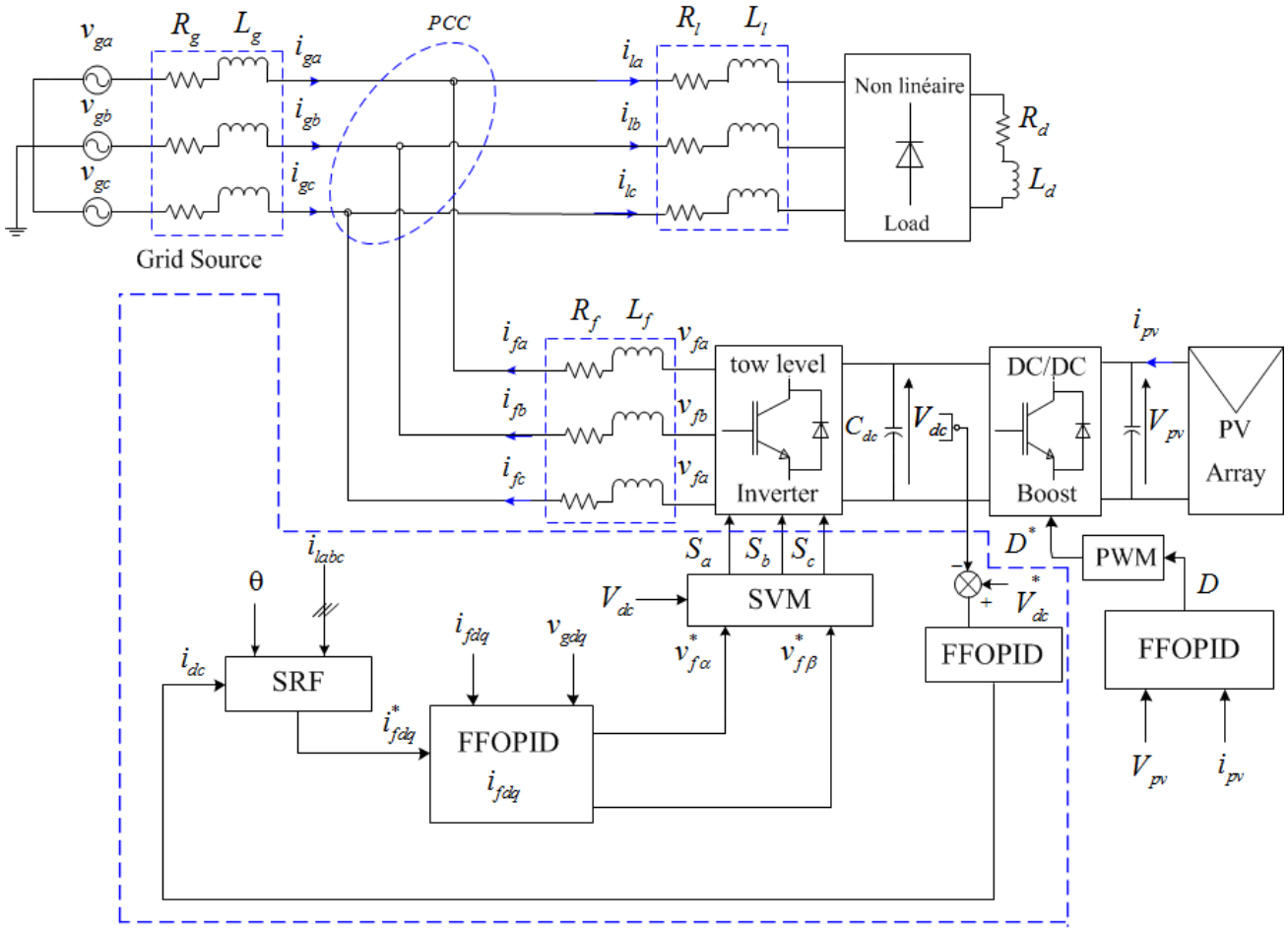

Figure 1. Power circuit diagram of the FFOPID for the PV-SAPF system

Table 1. Comparison of the proposed FFOPID-based control strategy with recent related works

Criteria	Proposed work FFOPID-based control	Ref. [41]	Ref. [42]	Ref. [43]	Ref. [44]
Main objective	Power quality improvement and harmonic mitigation	Microgrid energy management	Robust PV control with filtering	Power quality improvement	Robust PV–BESS control
System type	Grid-tied PV with SAPF	Microgrid with HESS	Grid-connected PV + filter	SAPF with 3-level VSI	PV + BESS with multifunctional VSI
Controller type	Fuzzy fractional-order PID (FFOPID)	NARX–RBF neural network	GA-based super-twisting SMC	Synergetic control	Integral backstepping + DPC-SVM
Intelligence/ Adaptivity	Fuzzy logic–based	AI / data-driven	Optimization-based	Model-based nonlinear	Model-based nonlinear
Fractional-order control	Yes	No	No	No	No
Active power filtering	Yes (Integrated)	No (energy management focused)	Yes	Yes	Partial
DC-link voltage regulation	Excellent (low ripple)	Not primary focus	Good (with oscillations)	Moderate	Good
Power ripple	Very low	Not reported	Moderate	Moderate	Moderate
Grid current THD (%)	≈ 0.6%	Not reported	≈ 2–4%	≈ 3–5%	≈ 2–4%
Power factor	Unity	Unity	Unity	Unity	Unity
Robustness to disturbances	High (irradiance, load, parameters)	High (load/storage variation)	High (but chattering-prone)	Moderate	High (model-dependent)
Computational complexity	Moderate	High	High	Low–moderate	moderate
Main advantages	Very low THD, smooth response, no chattering, robust	Effective energy management	Strong robustness	Simple nonlinear control	Accurate dynamic control
Main limitations	Tuning complexity of FFOPID	Requires training data	Chattering and tuning burden	Limited adaptivity	Strong dependence on model accuracy
Overall contribution	State-of-the-art power quality enhancement with low THD	Advanced EMS for microgrids	Robust nonlinear PV control	SAPF performance improvement	Multifunctional PV–BESS control

2.1 DC-DC boost converter modeling

Equation (1) presents the dynamic equations that define the state-space model of the converter, as described in [45].

$$\begin{cases} \dfrac{dV_{pv}}{dt} = \dfrac{1}{C_{pv}} i_{pv} - \dfrac{1}{C_{pv}} i_l \\ \dfrac{di_l}{dt} = \dfrac{1}{L}(1 - D_{pv}) V_{pv} - \dfrac{1}{L_{pv}} V_{dc} \end{cases} \tag{1}$$

2.2 SAPF modeling

The differential equations describing the dynamic mathematical model of the three-phase SAPF in the dq reference frame are given as follows [45, 46].

$$\begin{cases} \dfrac{di_{fd}}{dt} = -\dfrac{R_f}{L_f} i_{fd} + \dfrac{1}{L_f} v_{fd} - \omega i_{fq} - \dfrac{1}{L_f} v_{gd} \\ \dfrac{di_{fq}}{dt} = -\dfrac{R_f}{L_f} i_{fq} + \dfrac{1}{L_f} v_{fq} + \omega i_{fq} - \dfrac{1}{L_f} v_{gq} \\ \dfrac{dV_{dc}}{dt} = \dfrac{1}{C_{dc}} i_{dc} \end{cases} \tag{2}$$

3. THE PROPOSED FFOPID TECHNIQUE

Usual PID regulators may prove insufficient for handling complex systems. To address this, a fractional-order regulator is proposed as an alternative to improve system performance. The fractional order PID (FOPID) controller, represented as ($PI^{\delta}D^{\mu}$), is described in the time domain as follows [47, 48].

$$u(t) = k_p e(t) + k_i D^{-\delta} e(t) + k_d D^{\mu} e(t) \quad (3)$$

In this context, e(t) represents the error signal, while $u(t)$ denotes the command signal. The proportional gain is K_p, the integral gain is K_i, and the derivative gain is K_d. The parameters δ and μ correspond to the non-integer orders of the integral and derivative components, respectively [49, 50].
With:

$$e(t) = X^* - X \quad (4)$$

The operator D^{α} signifies the generalized fractional derivative/integral of order α, typically described using the Riemann Liouville definition, as follows:

$${}_aD_t^{\alpha} f(t) = \frac{1}{\Gamma(n-\alpha)} \frac{d^n}{dt^n} \left[\int_a^t \frac{f\tau}{(1-\tau)^{a-n+1}} d\tau \right] \quad (5)$$

Here, n is an integer that satisfies the condition $n-1 < \alpha < 1$, Γ (.) denotes the Euler gamma function, and a and t represents the limits of integration. The Laplace transform of Equation (6), assuming zero initial conditions, is given as follows:

$$L_a \left\{ D_t^{\alpha} f(t) \right\} = \int_0^{\infty} e^{-st} {}_aD_t^{\alpha} f(t) dt = s^{\alpha} F(s) \quad (6)$$

The FLC technique has emerged as a highly significant strategy in control systems, valued for its robustness and ease of application, as it does not require an understanding of the mathematical model of the system being studied [51]. FLC places considerable emphasis on user experience and logical reasoning, employing rules as opposed to binary values (0 and 1). The fundamental underpinnings of the FLC technique are constituted by three core principles: fuzzification, the inference engine, and defuzzification. This technique has been successfully applied across various fields [52, 53], yielding very satisfactory results. In [52-54], the FL technique was integrated with a GA to control a doubly-fed induction generator, demonstrating notable improvements in both the performance of the FLC technique and the overall system. In [55], the author introduced a novel FL-based approach to ensure the smooth operation of power systems during outages of RE sources and fluctuations in load demands. This algorithm is recognized for its robustness and its ability to enhance load frequency control (LFC). The proposed method utilizes a cascade fuzzy non-integer (fractional-order) proportional-derivative control in conjunction with a filter-proportional integral (CFPDlF-PI) approach to address frequency anomalies caused by the integration of renewable generation units within the existing power system.
To ascertain the proposed controller parameters, a slime mold algorithm was utilized. A series of tests was conducted to assess the performance of this control in enhancing the system's characteristics. The collected data indicate that the new approach is highly effective in enhancing the studied power system, as evidenced by significant performance metrics. As posited by Reference [56, 57], the employment of a fuzzy-tilt-fractional-order integral filtered derivative (FTIkDN) controller emerges as a pioneering instrument capable of augmenting the automatic generation control of multi-area interconnected power systems. The FLC method employed involves the strategic design of membership functions (MFs) near zero for fine-tuning, and those further from zero for coarse-tuning. This approach utilizes asymmetrically spaced MFs, a key component of the method. The imperialist competitive algorithm was implemented to calculate the proposed control parameters, resulting in enhanced outcomes and performance. This strategy was implemented, and a real-time hardware-in-the-loop (HIL) simulation test was performed to validate the method's feasibility and efficacy for practical applications. The validity of this proposed approach is substantiated by a comparative analysis of the results obtained with those of several existing controllers.
In this work, Membership functions were used as shown in Figure 2. Seven functions were tested to implement this FLC to achieve high operational performance, fast dynamic response, and high robustness. Furthermore, using seven functions allows the system to have a low memory footprint, utilizing 49 rules as listed in Table 2.

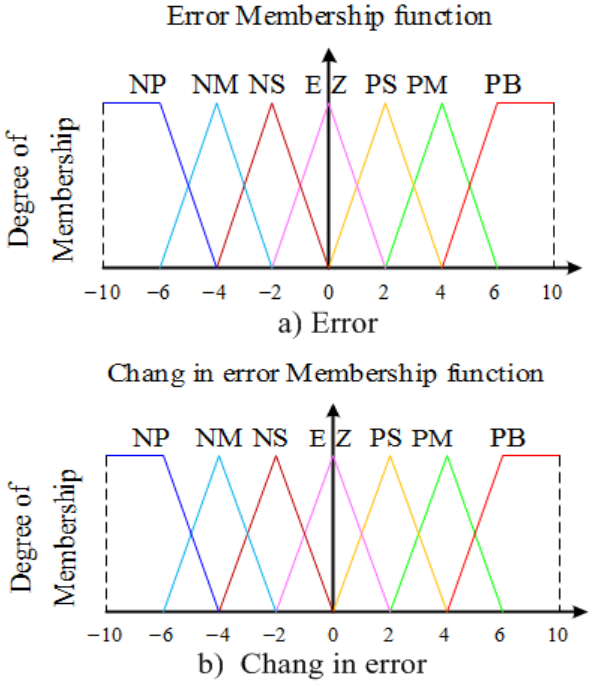

Figure 2. Membership functions (MFs).

Table 2. FL rules.

E Δe	NP	NM	NS	EZ	PS	PM	PB
NS	NB	NB	NM	NS	EZ	PS	PM
PS	NM	NS	EZ	PS	PM	PB	PB
NM	NB	NB	NB	NM	NS	EZ	PS
NB	NB	NB	NB	NB	NM	NS	EZ
PB	EZ	PS	PM	PB	PB	PB	PB
EZ	NB	NM	NS	EZ	PS	PM	PB
PM	NS	EZ	PS	PM	PB	PB	PP

Equation (7) expresses the proposed idea for the new organizer.

$$u(t) = fuzzy\ (e(t)) = fuzzy(X^* - X) \quad (7)$$

In this section, a novel controller is developed by combining the FLC with FOPID. The merits of this controller are notable for its robustness, simplicity, ease of implementation, and ease of response tuning. The FFOPID controller is a synthesis of two distinct control strategies, each with its own unique principles and advantages. The novel controller is delineated by Equation (8).

$$u(t) = \left(fuzzy\ (e(t))\right)\left(k_p e(t) + k_i D^{-\delta} e(t) + k_d D^{\mu} e(t)\right) \quad (8)$$

The gains of the controller designed in this study were calculated using a genetic algorithm. This algorithm was chosen for its simplicity and ease of implementation using MATLAB, as it does not require writing a complex program or knowing the mathematical model of the system under study. The Integral of Time-weighted Absolute Error (ITAE) was used to implement the genetic algorithm.

4. FFOPID STRATEGY APPLIED TO SAPF

4.1 current control loops (i_{fd} and i_{fq})

In this section, the SAPF command is developed using the FFOPID technique. The goal of this algorithm is to regulate the DC voltage V_{dc} and ensure that the active filter currents i_{fd} and i_{fq} closely follow their respective reference values. In the proposed approach, both parameters are regulated by the FOPID. The tuning process for the FFOPID involves the introduction of a series of static manifolds, which are designed to address system-specific challenges, such as power ripples and current degradation. This approach is particularly effective in cases where system parameters change or malfunctions occur. The subsequent step entails a systematic decomposition of the original dynamic system. One of the preliminary stages in implementing the SC, consistent with ADAR's methodology, entails the precise identification of the error to be addressed. This involves a focus on issues such as power oscillations and current, while taking into account the physical dynamics of the processes occurring within the system under investigation.

The initial step in the design process is the identification of the error. The following FFOPID functions have been meticulously engineered to establish the desired trajectory for the electric current.

$$\begin{cases} e_{i_{fd}} = i_{fd}^* - i_{fd} \\ e_{i_{fq}} = i_{fq}^* - i_{fq} \end{cases} \quad (9)$$

The FFOPID controllers are used to regulate the active filter's current, as demonstrated in Equations (10).

$$\begin{cases} u_d = A(a + b + c) \\ u_q = A'\left(a' + b' + c'\right) \end{cases} \quad (10)$$

With: $A = fuzzy\ (e_{i_{fd}})$, $a = k_{p_{i_{fd}}} e_{i_{fd}}$,

$b = k_{i_{i_{fd}}} D^{-\delta_{i_{fd}}} e_{i_{fd}}$, and $c = k_{d_{i_{fd}}} D^{\mu_{i_{fd}}} e_{i_{fd}}$

$A' = fuzzy\ (e_{i_{fq}})$, $a' = k_{p_{i_{fq}}} e_{i_{fq}}$, $b' = k_{i_{i_{fq}}} D^{-\delta_{i_{fq}}} e_{i_{fq}}$,

and $c' = k_{d_{i_{fq}}} D^{\mu_{i_{fq}}} e_{i_{fq}}$

After calculating the voltages u_d and u_q, the voltages v_{fd}^* and v_{fq}^* can be determined using Equations (11).

$$\begin{cases} v_{fd}^* = u_d + L_f \omega i_{fq} + v_{gd} \\ v_{fq}^* = u_q + L_f \omega i_{fd} + v_{fq} \end{cases} \quad (11)$$

4.2 DC link voltage control loop

In this section, the current i_{dc} is identified as the command variable, while the voltage V_{dc} is considered the input variable.

We define the switching error as follows:

$$e_{V_{dc}} = V_{dc}^* - V_{dc} \quad (12)$$

The FFOPID controller manages the DC bus voltage of the APF, as indicated in Equation (13).

$$i_{dc} = E\left(e_1 + e_2 + e_3\right) \quad (13)$$

With: $E = fuzzy\ (e_{V_{dc}})$, $e_1 = k_{p_{V_{dc}}} e_{V_{dc}}$,

$e_2 = k_{i_{V_{dc}}} D^{-\delta_{V_{dc}}} e_{V_{dc}}$, and $e_3 = k_{d_{V_{dc}}} D^{\mu_{V_{dc}}} e_{V_{dc}}$

5. FFOPID STRATEGY APPLIED TO DC-DC-BC

The FFOPID regulator-based control strategy is employed for the DC-DC-BC to optimize power extraction from the PV generator. As demonstrated in Figure 1, the FFOPID control law necessitates the development of both equivalent control and switching control. To achieve this objective, it is imperative to design a suitable sliding surface. Among the various

surface design methods, the error-based design method has been selected. The PV array's characteristics are the foundation for the subsequent mathematical representation, which is derived for operation at the MPPT [20]:

$$V_{pv}\frac{\partial i_{pv}}{\partial V_{pv}}+i_{pv}=0 \quad (14)$$

The definition of the error is a critical step in regulating the FFPID. The error for the PV cells is defined as follows:

$$e_{P_{pv}}=V_{pv}\frac{\partial i_{pv}}{\partial V_{pv}}+i_{pv}=0 \quad (15)$$

The FFOPID control can be expressed as follows:

$$D_{pv}=C\left(c_1+c_2+c_3\right) \quad (16)$$

With: $C=u_{pv}\left(fuzzy\left(e_{P_{pv}}\right)\right)$, $c_1=k_{p_{P_{pv}}}e_{P_{pv}}$,

$c_2=k_{i_{P_{pv}}}D^{-\delta_{P_{pv}}}e_{P_{pv}}$, and $c_3=k_{d_{P_{pv}}}D^{\mu_{P_{pv}}}e_{P_{pv}}$

6. STABILITY STUDY

This section examines the stability of the approach designed using the Bode curve. The Bode curve was chosen because it is easily obtained from MATLAB without requiring complex calculations. Figure 3 shows the Bode curve for two controls. The numerical results obtained from the Bode curve are listed in Table 3. According to Figure 3, the Phase value for both controls takes negative values, as its value changes with the frequency. Furthermore, Figure 3 shows that the Magnitude value also changes with the frequency and takes negative values when both controls are used. The frequency-domain stability analysis based on the Bode criterion highlights a clear quantitative improvement achieved by the proposed FFPID controller. For the conventional PI regulator, the phase at the gain crossover frequency is approximately −140°, resulting in a phase margin of about 40°. In contrast, the FFPID controller exhibits a phase of nearly −100° at the same criterion, yielding a significantly larger phase margin of approximately 80°. Moreover, at the phase crossover frequency (−180°), the magnitude of the open-loop response is around −10 dB for the PI regulator, corresponding to a gain margin of nearly 10 dB. Conversely, the proposed FFOPID controller presents a much lower magnitude of approximately −60 dB at −180°, which translates into a gain margin of about 60 dB, or practically infinite in some operating ranges. According to classical control theory, such substantial increases in both phase and gain margins indicate a higher robustness against gain variations, model uncertainties, and external disturbances, thereby confirming the superior closed-loop stability of the proposed FFPID regulator.

Table 3. Numerical results of the Bode curve when using the two controls

Features	PI controller	Proposed FFOPID controller
Gain crossover frequency, ω_{gc}	Lower	Higher
Phase at ω_{gc} (deg)	≈ −140°	≈ −100°
Phase Margin (PM)	≈ 40°	≈ 80°
Phase crossover (−180°)	Occurs	Occurs at much lower magnitude or does not occur
Magnitude at −180° (dB)	≈ −10 dB	≈ −60 dB
Gain Margin (GM)	≈ 10 dB	≈ 60 dB / Infinite
Overall stability	Stable	Highly stable

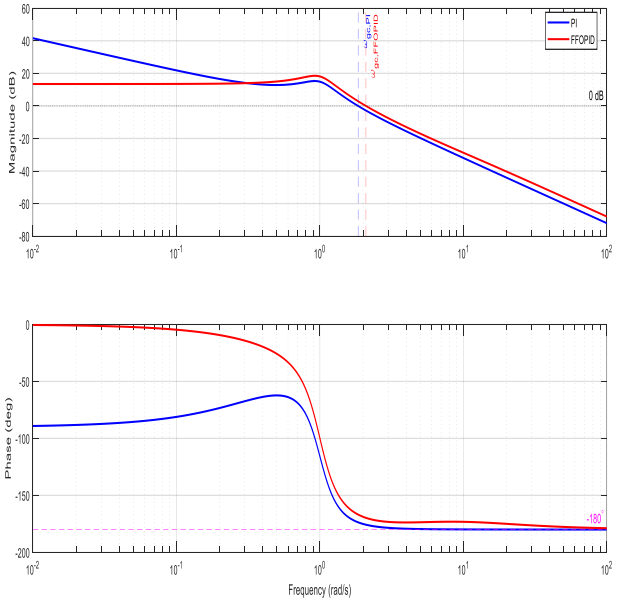

Figure 3. Bode curve of the designed techniques.

7. RESULTS AND DISCUSSION

This section presents the simulation of the designed system, comprising a PV system integrated with a SAPF. The parameters used for system implementation are listed in Table 4. A performance comparison between the PI and FFOPID controllers is conducted, with a focus on system enhancements and key characteristics. The simulation outcomes, inclusive of graphical representations, are displayed in Figures 4-14.

The parameters of the designed approach extracted using the genetic algorithms are represented in Table 5. These parameters were used to extract the results using MATLAB.

Table 4. System parameters

SAPF	
Source voltage (Rms value) V_g	70 V
Grid frequency f_g	50 Hz
R_g	0.1 Ω
L_g	0.1 mH
R_l	0.01Ω
L_l	0.566 mH
R_d	40Ω
L_d	2. 10 mH
Output filter resistance (*Rf*)	0.01 Ω
Output filter inductance (*Lf*)	2.5 mH
DC link capacitor (C_{dc})	2200 µF
DC link reference voltage (V_{dc})	226
Switching frequency (*f*)	20 kHz
PV Array	
V_{oc}	43.5 V
I_{sc}	4.75 A
V_{mp}	34.5 V
I_{mp}	4.35 A
P_{mp}	150 W
Ns	4
Np	2
DC-DC-BC	
C_{pv}	20 µF
Input inductor (*L*)	3 mH
Switching frequency (*f*)	20 kHz

Table 5. Parameters of the designed approach

Parameter	Description	Optimized Value
K_p	Nominal proportional gain	1.2
K_i	Nominal integral gain	0.30
K_d	Nominal derivative gain	0.05
δ	Fractional order integral	0.90
µ	Fractional order derivative	1.10
μK_p	Fuzzy proportional modulation gain	0.40
μK_i	Fuzzy integral modulation gain	0.12
μK_d	Fuzzy derivative modulation gain	0.02
SF_e	Fuzzy error scaling factor	1.0
SF_{de}	Fuzzy error derivative scaling	0.10
SF_{out}	Fuzzy output scaling factor	2.0

A. First Test

The FFOPID controller is assessed under varying solar radiation (SR) and non-linear load conditions to compare its performance with other control strategies.

Figure 4 illustrates the SR profile utilized in the simulation (Test 1), which is divided into six stages, each lasting 0.3 seconds. The SR levels were measured at 900 W/m², 600 W/m², 250 W/m², 800 W/m², 1000 W/m², and 100 W/m², respectively, over the time intervals [0s to 0.4s], [0.4s to 0.8s], [0.8s to 1.2s], [1.2s to 1.6s], [1.6s to 2.4s], and [2.4s to 2.8s]. Furthermore, Figure 5 illuminates the alterations in the non-linear load during the designated time intervals: [0s to 1.6s], [1.2s to 2s], [2s to 2.4s], and [2.4s to 2.8s].

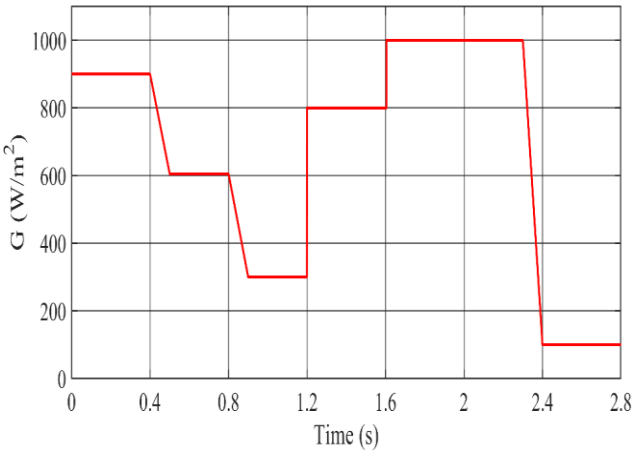

Figure 4. Irradiation profile.

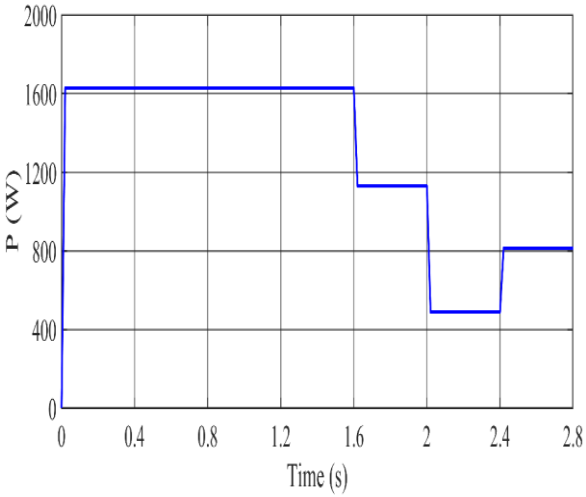

Figure 5. Non-linear load changes.

Figure 6 shows the relationship between the current (i_{pv}) and power (P_{pv}) produced by the PV generator in response to different levels of solar irradiation (G). Initially, before t = 0.4s, current or energy is created at a solar irradiation level of 900 W/m², 8 A, and 1,100 W. Between 0 and 0.8s, the solar irradiation level gradually increases to 600 W/m², resulting in the generation of 5.3 A and 750 W using the FFOPID. From 0.8 to 1.2 seconds, the irradiation decreases from 600 to 250 watts per square meter (W/m²), causing the current to drop from 5.3 amperes (A) to 2.3 A and the power to decline from 750 W to 260 W.

From 1.2 to 1.6 seconds, the irradiation decreases further, from 250 to 800 W/m², reducing the current from 2.3 A to 7 A and the power from 260 W to 970 W.
From 1.6 to 2.4 seconds, the irradiation increases again, reaching 1000 W/m² and stabilizing at this level. It provides 1200 W with an output of 8.9 A. Finally, from 2.4 to 2.8 seconds, the irradiation decreases to 100 W/m², maintaining this level and delivering 100 W with a current of 0.8 A.

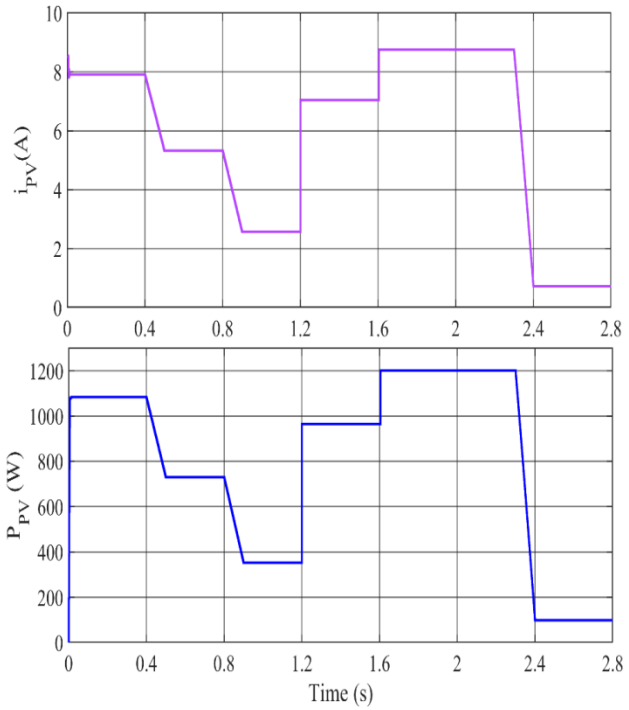

Figure 6. Power and current of the GPV.

Figure 7 illustrates energy flow management in a PV grid-connected system under varying load demands and irradiance profiles. For simulation purposes, the operation of the hybrid energy system is divided into six distinct states: States 1 through 6. Each state has different load energy consumption values and varying SR conditions.
Case 1: It can be seen that between t = 0 and 0.4s, when there is irradiance 900 W/m², the grid provides about 500 W of power and PV 1100 W. The majority of this, around 1655 W, is consumed by the non-linear load, while the remaining power compensates for APF losses, ensuring the DC bus voltage remains stable. This situation is expressed by the equation $P_L = P_g+P_{pv}$, where P_{PV} is less than P_g.
Case 2: Between t = 0.4 and 0.8s, the PV system generates approximately 750 W of power, while the grid supplies 900 W, reflecting the updated temperature and irradiation profile. The non-linear load, which consumes 1655 kW, is the main user of this energy, with the remainder used to offset the APF losses and maintain a stable DC bus voltage. This relationship is expressed by the equation $P_L = P_{PV}+P_g$, where P_{PV} exceeds P_g.
Case 3: The same case 2.
Case 4: The same case 3.
Case 5: From 2 to 2.4s, the PV system generates 1200 W, nearly matching the load demand of 1170 W. During this time, the utility grid supplies no power, leading to the relationship $P_L = P_{PV}$ and $P_g = 0$.
Case 6: From 2 to 2.4s, the PV system produces 1200 kW, which surpasses the load demand of 500 W. As a result, 700 W of surplus energy is supplied to the grid, indicating that P_{PV} is greater than P_L.
Case 7: Between t = 2.4 and 2.8s, the load power is 730 W, while the PV power drops to 100 W. During this phase, the non-linear load is powered by both the PV system and the grid, with the grid contributing 610 W. The total power supplied to the load is the sum of these two sources, expressed as $P_L = P_{PV}+P_g$, where PPV is less than P_g.

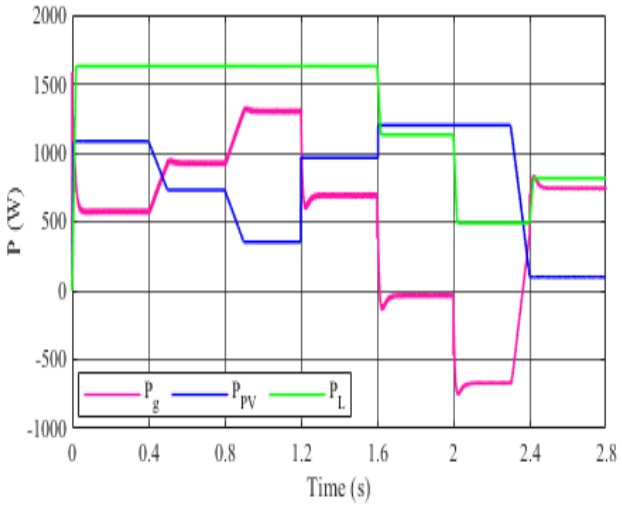

Figure 7. Energy flow management.

As illustrated in Figure 8, the DC link voltage for the two regulators utilized in this study is presented. The figure indicates that the DC link voltage closely follows the reference for all controllers, despite occasionally exceeding the limit value. This overshoot is more pronounced with the PI regulator compared to the other regulators (FFOPID). The PI regulator demonstrates superior responsiveness for direct current connections, a phenomenon that can be attributed to its inherent simplicity and seamless implementation. However, there are noted instances of the voltage exceeding the limit at 0.4s, 0.8s, 1.2s, 1.6s, and 2s, which are attributed to changes in solar irradiation and load. This finding suggests that the DC link voltage is susceptible to variations in SR. This effect manifested with greater significance in the PI compared to other regulators. However, the designed algorithms can be compared in both steady and transient states using the performance indicators

presented in Table 6. Table 6 shows that the FFOPID approach reduced the response time, SSE, overshoot, and undershoot of DC link voltage by 75%, 73.86%, 56.52%, and 50%, respectively, compared to the PI-based approach. These percentages demonstrate the effectiveness of the FFOPID controller and its ability to significantly improve the characteristics of the system under study, making it a viable option for wind turbines.

Table 6. Performance indicators values

Methods	Response time (s)	SSE (V)	Overshoot (V)	Undershoot (V)
FFOPID	0.05	0.23	5	6
PI	0.2	0.88	11.5	12
Ratios	75%	73.86 %	56.52%	50%

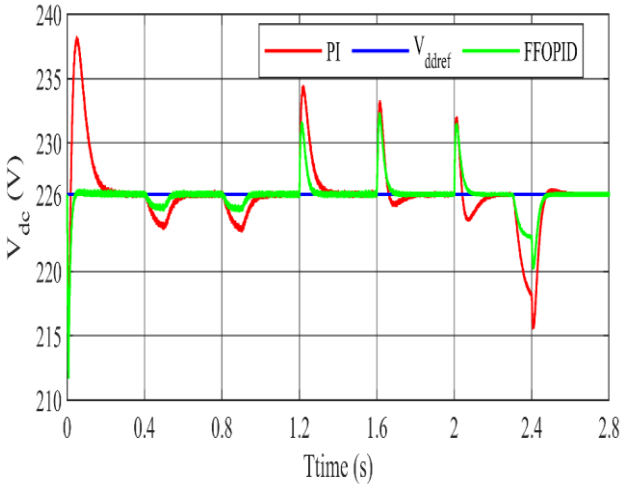

Figure 8. DC voltage with FFOPID and PI control.

As illustrated in Figure 9, the waveforms of the instantaneous real power at the source are presented. The proposed control method has been demonstrated to enhance dynamic performance by significantly reducing energy oscillations during SSE. The FOTOSMC technique has been demonstrated to maintain nearly continuous real power with minimal oscillations. In contrast, the PI controller has been shown to introduce more noticeable fluctuations in real power.

As illustrated in Figure 10, the *Qs* on the grid side remain at a constant zero for both control methods, thereby validating the earlier observation concerning the power factor. However, the FFOPID method demonstrates a reduced degree of fluctuation around zero in comparison to the alternative control method.

Figure 11 represents the performance of a system controlled by FFOPID. This figure shows the variations in three-phase network voltages, network current, filter current, and load current. It is evident from this figure that the network voltages are alternating currents with a maximum value of 200 V. It is also observed that the network current is sinusoidal with minimal ripple, reaching a maximum value of 5 A. The load current 2.4 seconds prior is approximately 3 A with a nearly sinusoidal shape, and after 2.4 seconds, its value increases to 5 A. Figure 12 shows the performance of a system regulated by PI control. In this figure, the network voltage exhibits a sinusoidal pattern with more ripples compared to the designed approach (Figure 11). Similarly, the network current also exhibits a sinusoidal pattern with ripples. These ripples are larger compared to the designed approach, where the maximum current value is 5 A, the same value achieved by the designed approach. Figure 12 also shows that the filter current before 2.4 seconds has a sinusoidal shape, but after this point, the current is no longer sinusoidal and exhibits larger ripples compared to the designed approach.

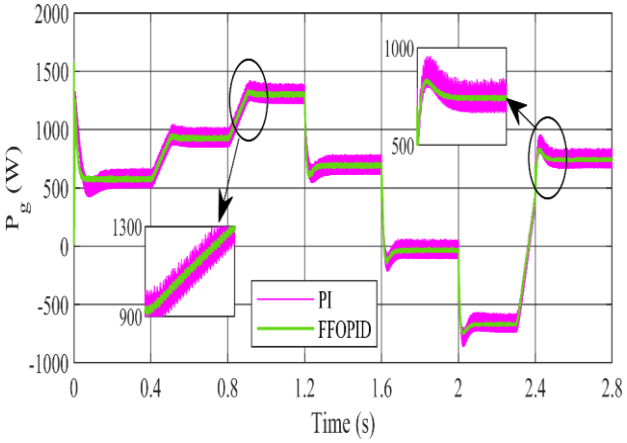

Figure 9. Grid active power.

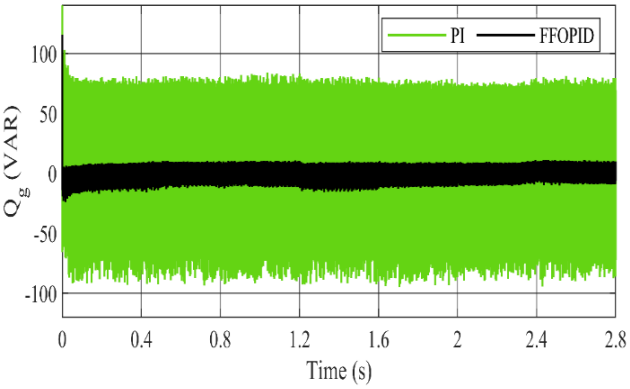

Figure 10. Grid imaginary power.

Figure 13 shows the THD value of the network current phase after filtering in the case of radiation equal to 100 W/m², using FFOPID control and PI control. The THD is 0.62% for FFOPID and 1.33% for PI in this scenario [2.4s to 2.8s]. These values indicate that the FFOPID regulator significantly reduced the THD value compared to the conventional regulator, with this reduction estimated at 53.38%. This percentage indicates that the current quality is high when using

the FFOPID regulator, making it a suitable choice in other industrial applications. On the other hand, the amplitude of the fundamental signal (50 Hz) at 100 W/m² was estimated to be 5 A and 5.002 A for FFOPID and PI, respectively. These values indicate that the two approaches yielded approximately the same amplitude.

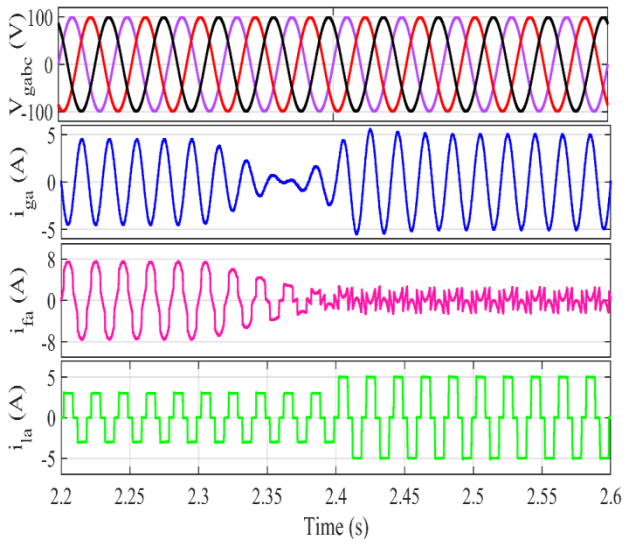

Figure 11. Performance of system controlled by FFOPID control.

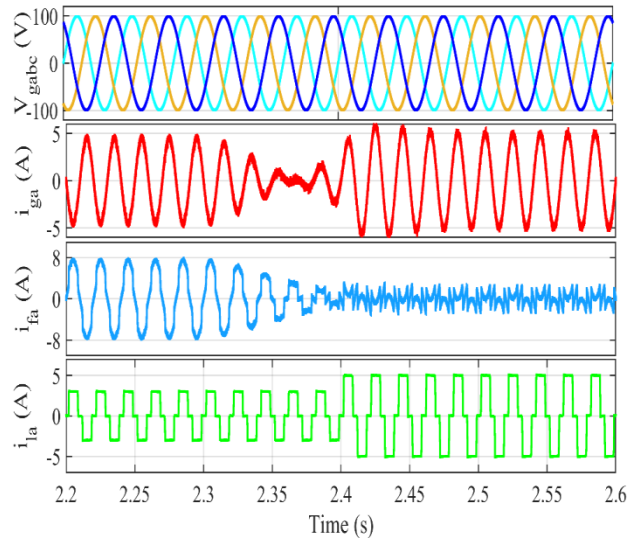

Figure 12. Performance of system regulated by PI control.

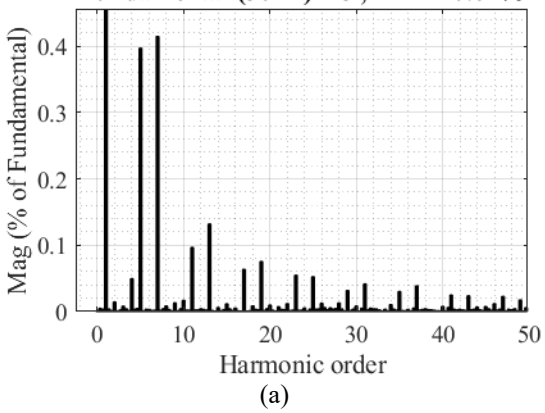

(a)

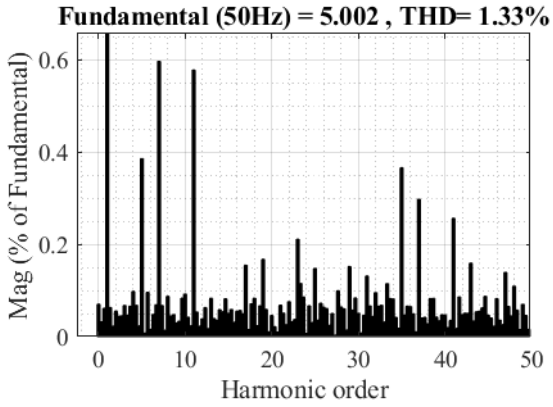

(b)

Figure 13. THD value of grid current: (a) FFOPID and (b) PI after filtration with PV system (100 W/m²).

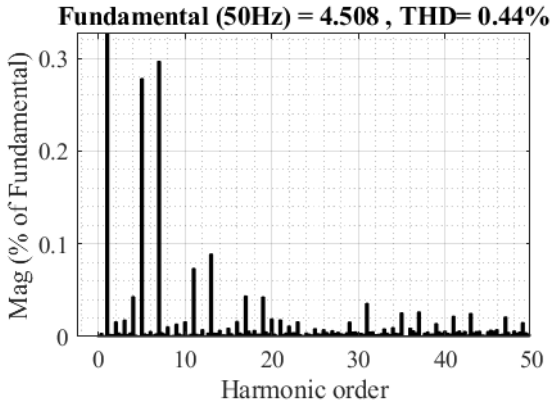

(a)

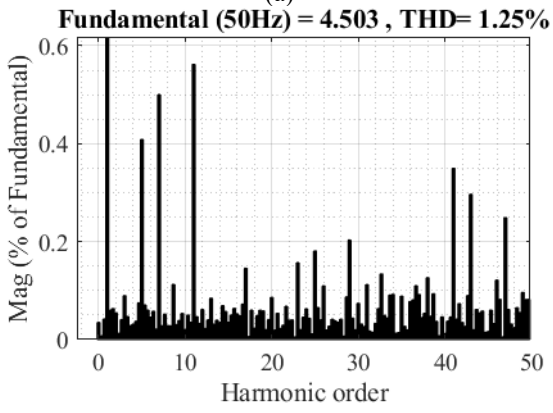

(b)

Figure 14. THD value of grid current: (a) FFOPID and (b) PI after filtration with PV system (1000W/m²).

Figure 14 represents the THD value for a current of 1000 W/m² using both control methods. This figure shows that the THD value is 0.44% when using the FFOPID algorithm and 1.25% when using the PI regulator. Figure 14 demonstrates that the THD value is significantly lower at 1000 W/m² when using the FFOPID approach, by approximately 64.80%, compared to the traditional strategy. Figure 14 also shows that the amplitude of the fundamental signal (50 Hz) was 4.508 A using the FFOPID approach and 4.503 A using the conventional approach. These

values indicate that the FFOPID approach provided larger amplitude compared to the conventional approach. These results demonstrate the effectiveness of the FFOPID approach in improving current characteristics and quality, making it a promising solution in the field of control.

The THD of the current is influenced by the radiation level for both PI and FOPID regulators, showing a slight improvement as radiation increases. When the radiation rises from 100 W/m² to 1000 W/m², the THD obtained with the PI regulator decreases from 1.33% to 1.25%, indicating marginally better current waveform quality at higher irradiance. A similar trend is observed with the FOPID regulator, where the THD reduces from 0.62% to 0.44% as radiation increases, reflecting enhanced harmonic suppression under higher power conditions. Overall, higher radiation levels lead to lower current THD for both command approaches, while the FOPID regulator consistently achieves significantly lower THD than the PI regulator across all radiation levels, demonstrating superior robustness and energy quality performance.

B. Robustness test

This test evaluates the robustness of the FFOPID regulator in comparison with the conventional PI regulator. To assess robustness, the system parameters are modified by increasing the grid resistance R_g and inductance L_g by 50% relative to their nominal values. Figure 15 illustrates the DC-link voltage responses of the two regulators considered in this study. The results indicate that the DC-link voltage generally follows the reference value for both controllers, although occasional overshoots beyond the allowable limit are observed. These voltage deviations are more pronounced when the PI regulator is employed compared to the FFOPID regulator. While the PI regulator demonstrates a faster transient response in DC-link voltage regulation—attributable to its simple structure and straightforward implementation—it also exhibits significant voltage overshoots at 0.4s, 0.8s, 1.2s, 1.6s, and 2s, corresponding to changes in solar irradiance and load conditions.

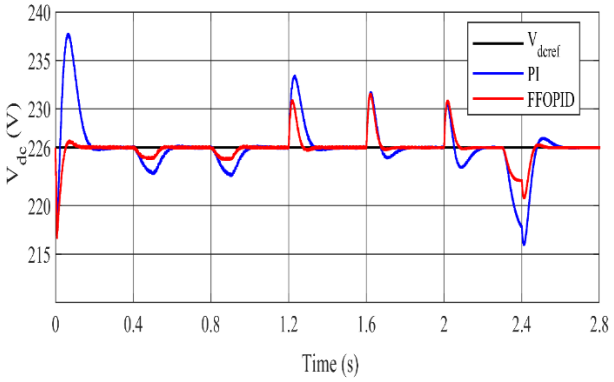

Figure 15. DC voltage with FFOPID and PI control.

These findings suggest that the DC-link voltage is sensitive to variations in solar irradiation, with this sensitivity being notably higher under PI control than with the FFOPID regulator, thereby highlighting the superior robustness of the FFOPID approach.

Figure 16 shows the instantaneous real power at the source. The results demonstrate that the proposed control strategy significantly enhances dynamic performance by effectively suppressing power oscillations during steady-state operation. In particular, the FFOPID-based approach maintains an almost constant real power profile with negligible fluctuations, whereas the PI controller exhibits comparatively larger oscillations.

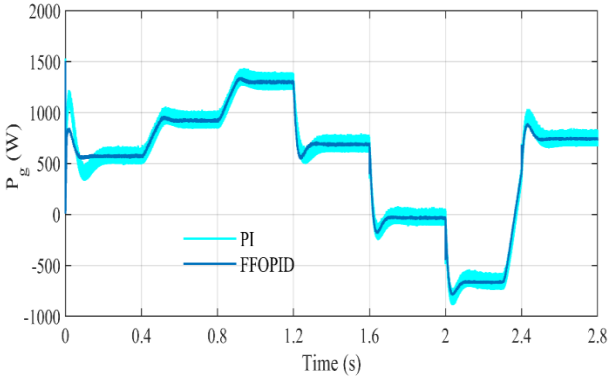

Figure 16. Grid active power.

As illustrated in Figure 17, the grid-side *Qs* remains close to zero for both control strategies, confirming operation at unity power factor. However, the FFOPID regulator shows smaller deviations around zero than the PI regulator, indicating improved *Qs* regulation.

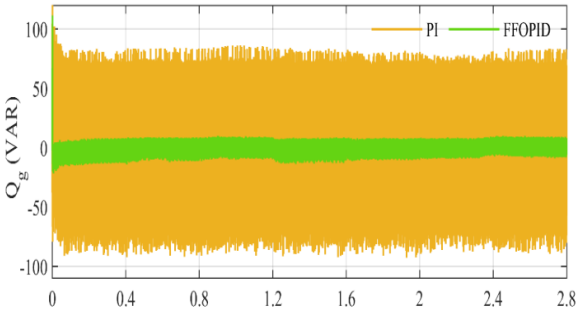

Figure 17. Grid imaginary power.

Figures 18 and 19 shows the THD value of the filtered single-phase network current when using FFOPID and PI regulators, respectively, when the radiation is equal to 100 W/m² and 1000 W/m². In the case of radiation equal to 100 W/m², the THD value was estimated at 0.61% when using the FFOPID regulator, while it was estimated at 3.92% when using the PI regulator. These values indicate that the FFOPID regulator reduced the THD value by approximately 84.43% compared to the conventional regulator. Furthermore, at a radiation level of 1000 W/m², the THD value was estimated at

4.05% with the conventional regulator and 0.63% with the FFOPID approach. Therefore, the FFOPID approach also yielded a significantly lower THD value compared to the conventional approach at a radiation level of 1000 W/m^2, highlighting its effectiveness and power in improving current characteristics. Accordingly, the FFOPID approach improved the THD value at a radiation level of 1000 W/m^2 by approximately 84.44% compared to the designed approach. Figures 18 and 19 show that the THD value in the designed approach increased by 3.17% with increasing radiation levels. However, the THD value in the conventional approach increased by 3.20%. Therefore, the designed approach exhibited a higher THD value change compared to the conventional approach. These results make the designed approach a promising option for other industrial applications, such as electric vehicles.

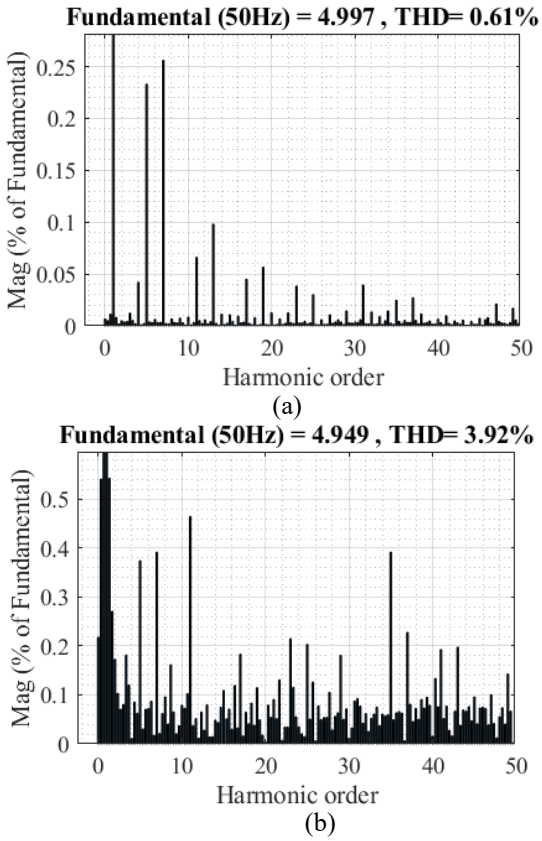

Figure 18. THD value of grid current: (a) FFOPID and (b) PI after filtration with PV system (100 W/m^2).

A comparative analysis was conducted between the new algorithm and several existing control methods within the same field, focusing on the current THD. The comparative results, shown in Table 7, clearly illustrate the superiority of the FFOPID, which achieves a lower THD compared to other command techniques, such as the backstepping command. Table 7 shows that the designed approach reduced the THD of current by 90.06% and 69.23% compared to work 58, and by 38.02% and 52.17% compared to [59] and [60], respectively. Furthermore, the designed approach reduced the THD by 61.46%, 82.60%, 80.09%, 66.66%, and 48.23% compared to [61], [62], [63], [64], and [65], respectively. These results indicate the high effectiveness and efficiency of the FFOPID approach compared to several strategies found in the literature in terms of improving current quality. This strong performance points to promising prospects for its future application in control systems, particularly in the renewable energy sector.

Table 7. Comparison in terms of THD value of the current.

Ratios	Algorithms	THD (%)	References
90.06%	PI control	4.43	[58]
69.23%	Simplified STA	1.43	
38.02%	H∞ regulators	0.71	[59]
52.17%	FLC	0.92	[60]
61.46%	Third-order SMC method	0.91	[61]
82.60%	SMC	2.53	[62]
80.09%	SC	2.21	[63]
66.66%	FO (PI + PD) cascade	1.32	[64]
48.23%	Fractional-order SC	0.85	[65]
Designed control strategy		0.44 (Test 1)	

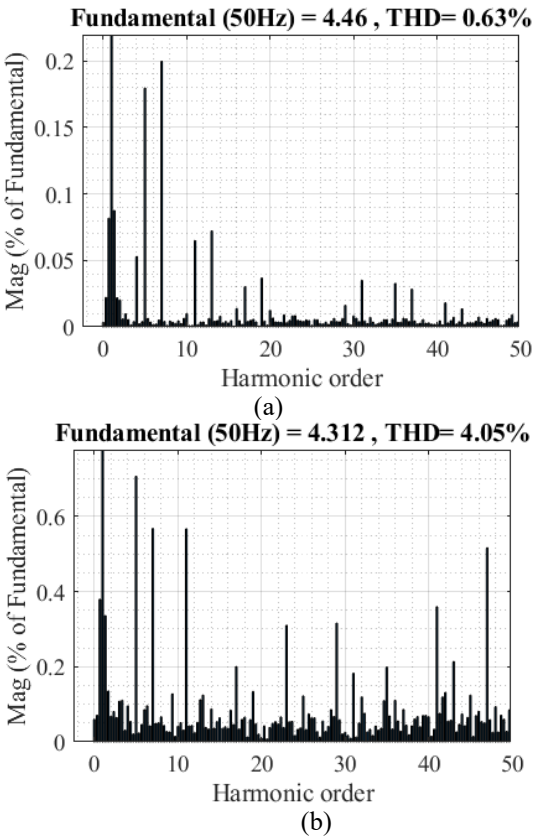

Figure 19. THD value of grid current: (a) FFOPID and (b) PI after filtration with PV system (1000W/m^2).

The simulation studies presented in this section confirm the effectiveness and robustness of the designed control strategy under various operating conditions, including variations in solar radiation, load variations, and parameter uncertainties. Comparative analyses with a usual control based on the PI regulator show that the designed approach achieves superior regulation of DC link voltage, reduced power fluctuations, improved reactive power compensation, and a significant reduction in current harmonic distortion. The results confirm stable operation at a power factor of one, with a fast dynamic response and improved power quality, highlighting the ability of the designed system to meet grid connectivity standards and practical deployment requirements.

8. CONCLUSIONS

This study examined a grid-connected PV power conversion system incorporating a parallel efficient power filter. Key contributions included coordinated control of PV energy injection and improved energy quality through harmonic mitigation and reactive power compensation. The FFOPID regulator was applied to both the enhanced DC-DC converter and the DC-AC converter to improve dynamic response and regulation performance. The simulation results show that the designed control strategy reduces the THD of the current and improves the power factor compared to a traditional PI regulator, while maintaining tracking of the maximum effective power point under varying operating conditions. These results demonstrate an improvement in both dynamic and static behavior within the simulated environment. However, the current findings are limited to numerical analysis and have not yet been experimentally verified.

Future work will focus on the experimental application of the proposed control approach using a miniaturized PV system to evaluate real-time performance, robustness, and operational limitations. Further studies will address the tuning of regulator parameters under network disturbances, such as voltage drops and frequency variations, as well as the impact of measurement noise and system nonlinearity. Extending this approach to include higher-capacity systems and comparing it with other advanced control technologies are important directions for further research.

NOMENCLATURE

PV	Photovoltaic system
PI	Proportional integral regulator
THD	Total harmonic distortion
PID	Proportional integral derivative regulator
FFPID	Fuzzy fractional-order proportional integral derivative regulator
WE	Wind energy
FOPID	Fractional-order proportional-integral derivative controller
VSI	Voltage source inverter
SSE	Steady-state error
SMC	Sliding mode controller
SC	Synergetic control
P&O	Perturb and observe
APF	Active power filter
ANN	Artificial neural network
PSO	Particle swarm optimization
GWO	Grey wolf optimization
YSGA	Yellow saddle goatfish algorithm
Qs	Reactive power
MPP	Maximum power point
DER	distributed energy resource
SAPF	Shunt active power filtre
MPPT	Maximum power point tracking
RE	Renewable energy
EP	Electrical power
PCC	Point of common coupling
STA	Super-twisting algorithm
VSC	Voltage source converters
DG	Distributed generation
IC	Incremental conductance
SCC	Short circuit current
OCV	Open circuit voltage
PWM	Pulse width modulation
FLC	Fuzzy logic control
GA	Genetic algorithm
Ps	Active power
PQ	Power quality

REFERENCES

[1] S. Devassy and B. Singh, "Performance Analysis of Solar PV Array and Battery Integrated Unified Power Quality Conditioner for Microgrid Systems," in IEEE Transactions on Industrial Electronics, vol. 68, no. 5, pp. 4027-4035, May 2021, doi: 10.1109/TIE.2020.2984439.

[2] S. Kadi, H. Benbouhenni, A. Yahdou, et al., "Performance optimization of wind turbines via fractional-order type 2 fuzzy MPPT control," Measurement and Control vol. 0, no. 0, pp. 1-25, 2025. Doi: 10.1177/00202940251398969.

[3] P. Shah, I. Hussain, and B. Singh, “Coordinated control of active power filter and photovoltaic inverter for power quality improvement in grid-tied systems,” *Int. J. Electr. Power Energy Syst*., vol. 135, pp. 107512, 2022, doi: 10.1016/j.ijepes.2022.107512.

[4] G. Ramesh, J. Logeshwaran, T. Kiruthiga, and J. Lloret, “Prediction of energy production level in large PV plants through auto-encoder based neural network with restricted Boltzmann feature extraction,” *Future Internet.,* vol. 15, no. 2, pp. 46, 2023, doi: 10.3390/fi15020046.

[5] B. Habib, et al., “Fractional-order synergetic control of the asynchronous generator-based variable-speed multi-rotor wind power systems,” in IEEE Access, vol. 11, pp. 133490-133508, 2024. doi: 10.1109/ACCESS.2023.3335902.

[6] H. Li et al., "Power Supply Reliability Enhancement for Low-Voltage Distribution Area With Power Quality Improvement Function," *in IEEE Access*, vol. 10, pp. 130619-130631, 2022, doi: 10.1109/ACCESS.2022.3229424.

[7] P. M. Reddy, B. K. Gupta and K. R. Sekhar, "Design and Implementation of Load Network Time Constant Computation Based Solar Active Power Filters Cum Injector for Industrial Loads/Grids," *in IEEE Access*, vol. 12, pp. 19967-19982, 2024, doi: 10.1109/ACCESS.2024.3361309.

[8] K. Hasan, M. M. Othman, S. T. Meraj, S. Mekhilef and A. F. B. Abidin, "Shunt Active Power Filter Based on Savitzky-Golay Filter: Pragmatic Modelling and Performance Validation," i*n IEEE Transactions on Power Electronics*, vol. 38, no. 7, pp. 8838-8850, July 2023, doi: 10.1109/TPEL.2023.3258457.

[9] S. M. Belhadj, B. Meliani, H. Benbouhenni, S. Zaidi, Z. M. S. Elbarbary, M. M. Alammer, "Control of multi-level quadratic DC-DC boost converter for photovoltaic systems using type-2 fuzzy logic technique-based MPPT approaches," Heliyon, vol. 11, no. 3, pp. e42181, 2025. https://doi.org/10.1016/j.heliyon.2025.e42181.

[10] A. Belhadj Djilali, A. Yahdou, E. Bounadja, et al., "Fuzzy Logic Based-Perturb and Observe Control with Energy Management for Photovoltaic-Battery and Diesel Hybrid System," *Arab J Sci Eng* vol. 50, pp. 5439–5461, 2025. https://doi.org/10.1007/s13369-024-09348-0.

[11] B. Abdelhakim et al., "Smart power conditioning unit utilizing enhanced INC–Con MPPT for photovoltaic power plants," *Int. J. Smart Grid*, vol. 8, no. 1, pp. 41–45, 2024, doi: 10.20508/ijsmartgrid.v8i1.330.g335.

[12] Kh. N. Khallouf, Z. Laid, B. Habib, N. Debdouche, Z. M. S. Elbarbary, "Adaptive fuzzy logic control for microgrid-connected hybrid photovoltaic/wind generation systems," Energy Reports, vol. 12, pp. 4741-4756, Dec 2024, https://doi.org/10.1016/j.egyr.2024.10.042.

[13] M. B. Bentrad, T. Bahi, and A. Boulassel, "Adaptive hybrid MPPT using artificial intelligence for an autonomous PV system," *Int. J. Smart Grid*, vol. 8, no. 1, pp. 27–34, 2024, doi: 10.20508/ijsmartgrid.v8i1.328.g331.

[14] F. Ouafia et al., "Optimized MPPT for aero-generator system using feed-forward neural network," *Int. J. Renew. Energy Res*., vol. 13, no. 3, pp. 1134–1144, 2023, doi: 10.20508/ijrer.v13i3.14002.g8785.

[15] K. D. Clément, H. K. Charles, and M. L. Bertrand, "Duty-cycle modulation and fuzzy controller for MPPT of a solar panel," *Int. J. Renew. Energy Res*., vol. 12, no. 1, pp. 70–80, 2022, doi: 10.20508/ijrer.v12i1.12628.g8374.

[16] M. A. Hannan et al., "Particle swarm optimization based fuzzy logic MPPT inverter controller for grid-connected wind turbine," *Int. J. Renew. Energy Res*., vol. 9, no. 1, pp. 164–174, 2019.

[17] A. S. Ahmed et al., "A fuzzy logic-based MPPT technique for PMSG wind generation system," *Int. J. Renew. Energy Res*., vol. 9, no. 4, pp. 1751–1760, 2019, https://doi.org/10.20508/ijrer.v9i4.10138.g7778.

[18] Y. Ishaque, T. Benbouhenni, and A. Larbes, "Analysis of genetic and cuckoo search algorithms for MPPT under partial shading," *Int. J. Smart Grid*, vol. 8, no. 1, pp. 35–40, 2024, https://doi.org/10.20508/ijsmartgrid.v8i1.329.g330.

[19] W. Cherif et al., "Energy management system for stand-alone multi-source grid using genetic algorithm," *Int. J. Renew. Energy Res*., vol. 13, no. 1, pp. 59–69, 2023, https://doi.org/10.1109/TPEL.2012.2185713.

[20] K. Ishaque et al., "An improved PSO-based MPPT for PV with reduced steady-state oscillation," *IEEE Trans. Power Electron*., vol. 27, pp. 3627–3638, 2012, doi: 10.1109/TPEL.2012.2185713.

[21] B. S. Goud and B. L. Rao, "Power quality improvement in hybrid renewable energy source grid-connected system with grey wolf optimization," *Int. J. Renew. Energy Res*., vol. 10, no. 3, pp. 1071–1082, 2020, doi: 10.20508/ijrer.v10i3.11318.g8004.

[22] H. Azli et al., "Novel yellow saddle goatfish algorithm for PV systems under partial shading," *Solar Energy*, vol. 247, pp. 295–307, 2022, doi: 10.1016/j.solener.2022.10.029.

[23] Y. Hoon et al., "Integrated I-ADALINE neural network and selective filtering techniques," *Symmetry*, vol. 17, pp. 1337, 2025, doi:10.3390/sym17081337.

[24] B. Condemaita and M. Ruiz, "Harmonic mitigation and energy savings in distribution feeders," *Energies*, vol. 18, pp. 5582, 2025, doi:10.3390/en18215582.

[25] M. I. M. Montero et al., "Comparison of control strategies for shunt active power filters," *IEEE Trans. Power Electron*., vol. 22, no. 1, pp. 229–236, doi: 10.1109/TPEL.2006.886616.

[26] A. Fereidouni and M. A. Masoum, "Adaptive space-vector hysteresis-based control," *Intell. Ind. Syst*., vol. 2, no. 4, pp. 319–334, 2016, https://doi.org/10.1007/s40903-016-0064-7.

[27] K. Swetha and V. Sivachidambaranathan, "Comparative analysis of DSTATCOM using PI and SOSMC," *in Proc. AI Evol. Comput. Eng. Syst*., 2020, pp. 193–203, 2020, doi: doi: 10.1007/s40903-016-0064-7.

[28] M. T. Benchouia et al., "Sliding mode and PI control of shunt active power filter," *Energy Procedia*, vol. 50, pp. 504–511, 2014, doi: 10.1016/j.egypro.2014.06.061.

[29] R. Arun and B. Ramkiran, "Shunt active power filter using hysteresis and PI control," *in Proc. IC-GET*, 2015, pp. 1–5, doi: 10.1109/GET.2015.7453860.

[30] S. Ahmad et al., "Chattering-free sliding mode control," *Electronics*, vol. 12, p. 876, 2023, doi: 10.3390/electronics12040876.

[31] E. Obukhova et al., "Synergetic synthesis of nonlinear throttle control laws," *Appl. Sci*., vol. 12, p. 1797, 2022, doi: 10.3390/app12041797.

[32] B. Habib, "A comparative study between DTC-NSTMC and DTC-FSTSMC control schemes for a DFIG-based wind turbine," *Majlesi J. Energy Manag*., vol. 7, no. 4, pp. 1–8, 2018, http://journals.iaumajlesi.ac.ir/em/index/index.php/em/article/view/370.

[33] B. L. Liu, Y. B. Zha, and T. Zhang, "Sliding mode control of solid-state transformer using a three-level hysteresis function," *J. Central South Univ*., vol. 23, no. 8, pp. 2063–2074, 2016, https://doi.org/10.1007/s11771-016-3262-2.

[34] S. Kadi et al., "A direct vector control based on modified sliding mode control for double-powered induction generator-based wind turbine systems," *Energy Rep*., vol. 8, pp. 15057–15066, 2022, https://doi.org/10.1016/j.egyr.2022.11.052

[35] H. Benbouhenni, F. Mehedi, and S. Laifa, "New direct power synergetic sliding mode control technique for DFIG-based wind power," *Automatika*, vol. 63, no. 4, pp. 718–731, 2022, doi: 10.1080/00051144.2022.2065801.

[36] H. Benbouhenni and N. Bizon, "Synergetic sliding mode controller applied to direct field-oriented control of induction generator-based wind turbines," *Energies*, vol. 14, no. 15, pp. 4437, 2021, doi: 10.3390/en14154437.

[37] H. A. Mosalam, R. A. Amer, and G. A. Morsy, "Fuzzy logic control for grid-connected PV array using Z-source inverter," *Ain Shams Eng. J*., vol. 9, no. 4, pp. 2931–2941, 2018, https://doi.org/10.1016/j.asej.2018.10.001.

[38] M. A. Hannan et al., "Fuzzy logic inverter controller in photovoltaic applications: Issues and recommendations," *IEEE Access*, vol. 7, pp. 24934–24955, 2019, doi: 10.1109/ACCESS.2019.2899610.

[39] T. Vigneysh and N. Kumarappan, "Grid interconnection of renewable energy sources using multifunctional converters," *Electr. Power Syst. Res*., vol. 151, pp. 359–368, 2017, doi: 10.1016/j.epsr.2017.06.010.

[40] H. M. Hasanien and M. Matar, "Fuzzy logic controller for autonomous operation of voltage source converter-based DG

system," *IEEE Trans. Smart Grid*, vol. 6, no. 1, pp. 158–165, 2015, doi: 10.1109/TSG.2014.2327398.

[41] Zaidi Sarra, Meliani Bouziane, Riyadh Bouddou, Habib Benbouhenni, Saad Mekhilef, Z.M.S. Elbarbary, "Intelligent control of hybrid energy storage system using NARX-RBF neural network techniques for microgrid energy management," Energy Reports, vol. 12, pp. 5445-5461, December 2024, https://doi.org/10.1016/j.egyr.2024.11.023.

[42] Naamane Debdouche, Laid Zarour, Ali Chebabhi, Noureddine Bessous, Habib Benbouhenni, Ilhami Colak, Genetic algorithm-super-twisting technique for grid-connected PV system associate with filter. Energy Reports, vol. 10, pp. 4231-4252, November 2023, https://doi.org/10.1016/j.egyr.2023.10.074.

[43] Brahim Deffaf, Hamoudi Farid, Habib Benbouhenni, Slimane Medjmadj, Naamane Debdouche, "Synergetic control for three-level voltage source inverter-based shunt active power filter to improve power quality," Energy Reports, Vol. 10, pp. 1013-1027, 2023, https://doi.org/10.1016/j.egyr.2023.07.051.

[44] N. Debdouche, L. Zarour, Habib Benbouhenni, F. Mehazzem, B. Deffaf, "Robust integral backstepping control microgrid connected photovoltaic System with battery energy storage through multi-functional voltage source inverter using direct power control SVM strategies," Energy Reports, Vol. 10, pp. 565-580, 2023, https://doi.org/10.1016/j.egyr.2023.07.012.

[45] B. Youcefa et al., "Backstepping direct power control for grid-connected PV system," *Adv. Model. Control*, vol. 74, no. 1, pp. 1–14, 2019, https://doi.org/10.18280/ama_c.740101.

[46] B. Deffaf et al., "Comparative analysis between backstepping, sliding mode and PI control applied to shunt active filter," *in Proc. 2nd Int. Conf. Adv. Electr. Eng. (ICAEE*), 2022, pp. 1–6, 2022, https://ieeexplore.ieee.org/document/9961971.

[47] E. Edet and R. Katebi, "On fractional predictive PID controller design method," *IFAC-PapersOnLine*, vol. 50, no. 1, pp. 8555–8560, 2017, https://www.sciencedirect.com/science/article/pii/S2405896317319626.

[48] N. Hamouda et al., "Optimal tuning of fractional-order PID controller using ant colony optimization," *J. Eur. Syst. Autom*., vol. 53, no. 2, pp. 157–166, 2020, https://doi.org/10.18280/jesa.530201.

[49] H. Gasmi et al., "Fractional-order PI super-twisting sliding mode controller for wind energy systems," *J. Power Electron*., vol. 22, no. 8, pp. 1357–1373, 2022, https://doi.org/10.1007/s43236-022-00430-0.

[50] R. Pradhan et al., "Optimal fractional-order PID controller design using ant lion optimizer," *Ain Shams Eng. J.*, vol. 11, no. 2, pp. 281–291, 2020, https://www.sciencedirect.com/science/article/pii/S2090447919301418.

[51] J. L. Azcue-Puma et al., "Fuzzy logic-based stator-flux-oriented direct torque control," *J. Control Autom. Electr. Syst*., vol. 25, no. 1, pp. 46–54, 2014, https://doi.org/10.1007/s40313-013-0091-5.

[52] M. Moallem et al., "Multi-objective genetic-fuzzy optimal design of PI controller," *IEEE Trans. Magn*., vol. 37, no. 5, pp. 3608–3612, 2001, https://doi.org/10.1109/20.952673.

[53] T.-C. Ahn et al., "Design of neuro-fuzzy controller on DSP for real-time induction motor control," *in Proc. IFSA–NAFIPS World Congr*., 2002, pp. 3038–3043, 2002, https://neuro.bstu.by/ai/To-dom/My_research/Review-DONE/Ukr-com-2007/FinalProgram.pdf#page=143.

[54] M. A. Khan, A. Merabet, and L. Liu, "Resilient fractional-order sliding mode control of hybrid active power filters," *Int. J. Electr. Power Energy Syst*., vol. 158, p. 109867, 2024, doi: 10.1016/j.ijepes.2023.109867.

[55] M. Singh et al., "Frequency stabilization using cascade noninteger fuzzy controller," *Energy Sources Part A*, vol. 44, no. 3, pp. 6213–6235, 2022, doi: 10.1080/15567036.2022.2046271.

[56] Y. Arya, "ICA-assisted fractional controller for AGC performance enhancement," *J. Ambient Intell. Humaniz. Comput*., vol. 14, no. 3, pp. 1919–1935, 2023, doi: 10.1007/s12652-022-04440-1.

[57] T. T. Nguyen et al., "Distributed cooperative control of heterogeneous active power filters," *IEEE Trans. Smart Grid*, vol. 15, no. 1, pp. 567–580, 2024, doi: 10.1109/TSG.2023.3290528.

[58] N. Debdouche et al., "Direct power control of three-level multifunctional VSI using super-twisting algorithm," *Energies*, vol. 16, pp. 4103, 2023, https://doi.org/10.3390/en16104103.

[59] S. Ouchen et al., "Robust DPC-SVM control strategy for shunt active power filter," *Int. J. Electr. Power Energy Syst*., vol. 117, p. 105699, 2020, https://doi.org/10.1016/j.ijepes.2019.105699.

[60] S. Musa et al., "Modified SRF-based shunt active power filter with fuzzy logic PWM," *Energies*, vol. 10, no. 6, p. 758, 2017, https://doi.org/10.3390/en10060758.

[61] D. Naamane et al., "Power quality improvement using third-order sliding mode DPC," *Iran. J. Sci. Technol. Trans. Electr. Eng*., vol. 47, pp. 1473–1490, 2023, https://doi.org/10.1007/s40998-023-00627-4.

[62] M. V. and A. Bhattacharya, "Peak power demand management using SMC-controlled SAPF," *IEEE Trans. Ind. Informatics*, vol. 17, no. 8, pp. 5270–5281, 2021, https://ieeexplore.ieee.org/search/searchresult.jsp?queryText=Peak+power+demand+management+SMC+controlled+SAPF.

[63] X. Chen et al., "Digital twin-assisted MPC for harmonic mitigation," *Appl. Energy*, vol. 350, p. 121756, 2023, https://doi.org/10.1016/j.apenergy.2023.121756.

[64] H. Nikkhah Kashani et al., "Optimal cascade non-integer controller for shunt active power filter," *Designs*, vol. 6, p. 32, 2022, https://doi.org/10.3390/designs6020032.

[65] B. Deffaf et al., "New control strategy for improving power quality of three-level T-type inverter," *Electronics*, vol. 12, p. 2117, 2023, https://doi.org/10.3390/electronics12122117